RSC Advances

PAPER

View Article Online
View Journal | View Issue

Cite this: *RSC Adv.*, 2021, **11**, 39278

Development of cellulose-based polymeric structures using dual functional ionic liquids†

Joana Galamba,[a] Vítor D. Alves,[b] Noémi Jordão *[a] and Luísa A. Neves *[a]

Received 24th April 2021
Accepted 17th October 2021

DOI: 10.1039/d1ra03204f

rsc.li/rsc-advances

Carboxylate ionic liquids (ILs) combining benzethonium (BE) and didecyldimethylammonium (DDA) as cations have been explored to be used for the first time as dual functional solvents for microcrystalline cellulose (MCC) dissolution and, subsequently development of polymeric structures. Considering that some ILs can remain in the polymeric structures after phase inversion, these ILs can offer advantages such as antibacterial/antimicrobial response and ability to disrupt H-bonds. In this context, all tested ILs have been able to dissolve MCC up to a concentration of 4% (w/w), resulting in different polymeric structures, such as gel-like or films, depending on the type of IL and the ratio between MCC and IL. Furthermore, FTIR spectroscopy showed that some IL remains in the polymeric structures, which can enhance their application in the biomedical field.

Introduction

Recently, several efforts have been made to replace materials obtained from non-renewable resources with more natural materials and thus, resources, especially due to the scarcity of fossil resources combined with the requirements for the use of environmental-friendly and sustainable processes.[1–4] In this context, cellulose is the most abundant polysaccharide found on earth, with outstanding properties such as biocompatibility, biodegradability, and thermal and chemical stability.[4,5] Cellulose is a highly crystalline linear polymer composed of repeated glucose units linked by β(1 → 4) glycosidic bonds, which form strong inter- and intramolecular hydrogen bond networks.[1,4–6] Considering that cellulose presents a complex structure as well as a high degree of polymerization (DP), the dissolution process is considered a critical step for its valorisation due to its insolubility in water and most conventional organic solvents.[3,4,6,7]

Nowadays, different existing technologies for dissolution and processing of cellulose are applied at industrial scale, however aggressive solvents, or processes, which present a threat to the environment, are used[6,8] namely "viscose process", which consists in the chemical functionalization of cellulose through its hydroxyl groups with carbon disulphide to produce xanthate esters[5,9] and "Lyocell process", which uses aqueous *N*-methylmorpholine-*N*-oxide (NMNO) as solvent.[5,9,10] Recently, Xu *et al.*[8] reported others examples of solvents or mixtures of solvents investigated for cellulose dissolution processes, such as aqueous cuprammonium or cupriethylenediamine hydroxide as aqueous non-derivatizing solvents,[11] DMSO/tetrabutylammonium fluoride (DMSO/TBAF) as non-aqueous non-derivatizing solvents,[11] *N*,*N*-dimethylformamide/N_2O_4 (DMF/N_2O_4) as aprotic derivatizing solvents,[11] LiCl/*N*,*N*-dimethylacetamide (LiCl/DMA) solvent,[12] $LiClO_4 \cdot 3H_2O$,[13] LiCl/dimethyl sulfoxide (LiCl/DMSO) solvent,[14] aqueous NaOH combined with urea[15] or thiourea[16] solvents, dimethyl sulfoxide/1,8-diazabicyclo-[5.4.0]-undec-7-ene (DMSO/DBU).[17] Despite their ability to dissolve cellulose, these solvents showed some disadvantages namely, high dissolution temperatures, instability, difficulty to be recovered, harsh processing conditions, lower cellulose dissolution ability, toxicity, or high cost.[1,8] In the last decades, ionic liquids (ILs),[1,4,18–22] and more recently, their analogous deep eutectic solvents (DES)[23–25] have gained increased interest as alternative solvents for cellulose dissolution and processing, which can be coupled with microwave and ultrasound technologies in order to increase their performance.[1] Indeed, ILs can be considered as non-derivatizing solvents to dissolve cellulose, without occurring chemical modification during dissolution process, through deconstruction of inter- and intramolecular hydrogen bonds networks (physical dissolution process).[26,27] However, they are not necessarily chemically inert and thus, both cation and anion can participate during the derivatization reactions or react with the dissolved polysaccharide.[28]

ILs are low-melting organic salts, conventionally with melting points below 100 °C, and usually, composed with a big, bulky organic cation and smaller organic or inorganic anion.[29,30] ILs gained much attention mainly due to their peculiar properties as well as the possibility to tune their final properties according to the adequate selection of cation and anion.[31] In general, ILs shows outstanding properties such as low vapour pressure, high chemical and thermal stability as well as they exhibit high ionic conductivity,

[a]*LAQV-REQUIMTE, Department of Chemistry, NOVA School of Science and Technology, Universidade Nova de Lisboa, 2829-516 Caparica, Portugal. E-mail: lan11892@fct.unl.pt; n.jordao@fct.unl.pt*

[b]*LEAF, Linking Landscape, Environment, Agriculture and Food, Instituto Superior de Agronomia, Universidade de Lisboa, Tapada da Ajuda, 1349-017 Lisboa, Portugal*

† Electronic supplementary information (ESI) available. See DOI: 10.1039/d1ra03204f

large electrochemical window, and excellent dissolution performance of organic, inorganic, and polymeric materials.[31] Nowadays, intensive studies related to the use of ILs in cellulose dissolution have been reported,[1,4,20,22,32,33] where indicate the ideal properties that ILs should have, namely lower water content, once water hinders with the dissolution process;[32,34] smaller cations as well as anions are preferred; and the hydrogen bond basicity (β), which is a H-bond accepting ability, conferred by the anion, should be high enough to establish strong intermolecular bonds with hydroxyl groups present in cellulose structure, leading to an improvement of its solubility.[32] The cellulose dissolution mechanism in ILs is based on the disruption of the hydrogen bonds between cellulose chains caused essentially by the interaction of the anion present in the IL with hydroxyl groups (OH) present in cellulose structure and the establishment of new hydrogen bonds.[1,22,35] Indeed, it is also suggested that the anions from the IL should be strongly basic enough to compete with the hydrogen bonds present in cellulose structure. However, the effect of the cation in the dissolution process is still unclear.[1,22,35] In this context, the most efficient anions for cellulose dissolution are halides (*e.g.* chloride, Cl^-), dialkylphosphate/dialkylphosphonate (*e.g.*, $[(EtO)_2PO_2]^-$) and carboxylates (*e.g.*, acetate $[OAc]^-$).[33]

Besides of dissolution and regeneration processes, functional ILs for homogeneous derivatization of cellulose, where all reagents including cellulose are completed dissolved, have been explored.[34] For example, dual functional ILs that can act as solvent as well as catalyst have been explored.[35] Recently, a melt-flowable thermoplastic was developed from forestry biomass through solvent-free acetylation, where a functionalizing agent derived from benzethonium chloride and sulfuric acid was used have been reported.[36]

In the last years, different works related to the cellulose dissolution with ILs and consequently, the development of cellulose-based materials such as gels[37–42] or aerogels,[43–46] blends,[47] composites[48,49] have been explored,[22] which can be applied in different fields, such as electrochemical sensors[50] and adsorption of heavy metals.[51]

In this context, the aim of this work consisted of the use of dual functional ionic liquids for dissolution of microcrystalline cellulose (MCC) and subsequently, development of valuable polymeric structures envisaged potential applications in the biomedical field. Considering that some fraction of ionic liquid can remain in the polymeric structure, even after several washes with water as non-solvent, the introduction of an additional functionality to IL structure, on the cationic part, can be advantageous to enhance their application. In this way, the ionic liquids have been designed to be capable to disrupt hydrogen bonds, such as short linear carboxylate anions are incorporated in IL structure but also have biological properties such as anti-bacterial or anti-microbial conferred by the cation counterpart. The selected cations and anions to prepare the desired ionic liquids are illustrated in Fig. 1.

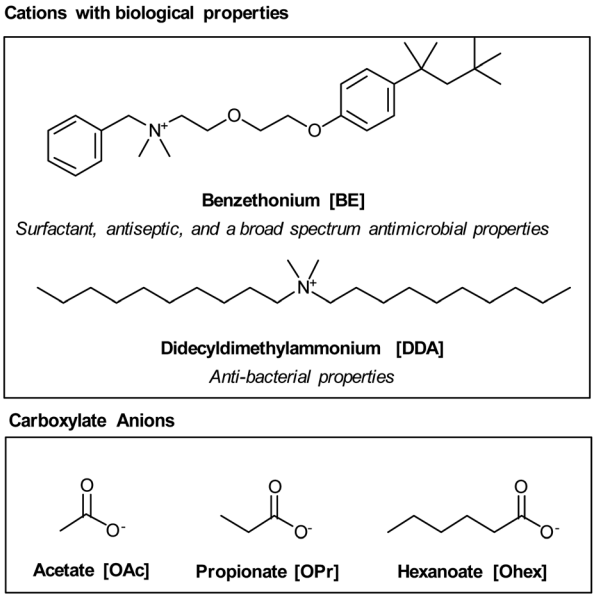

Fig. 1 Structure and respective acronyms of the selected cations and anions to develop dual functional ionic liquids, which has ability to disrupt hydrogen bonds and simultaneously possess a biological function, conferred by anion and cation, respectively.

Results and discussion

Synthesis and structural analysis of ILs

The selected synthetic methodology to prepare the desired ionic liquids consisted in two followed steps: (i) preparation of hydroxide form of the desired cation, through an anion exchange reaction using a ion exchange resin (Amberlyst A26 (OH))[52–54] and, subsequently, (ii) acid–base reaction using the selected carboxylate acid (acetic, propanoic, hexanoic) as illustrated in Scheme 1. This methodology has the advantage to prepare halide-free ILs, contrarily to the conventional metathesis reaction, which produces inorganic salts as by-product.[55]

All prepared ILs were analysed by ^1H, ^{13}C NMR and ATR-FTIR spectroscopies, and elemental analysis to check their structure and relative purity levels. From ^1H NMR and ^{13}C NMR spectra (see ESI-Fig. 1–12†), it was possible to assign typical signals of both cations[54,56] and anions, indicating that the desired product

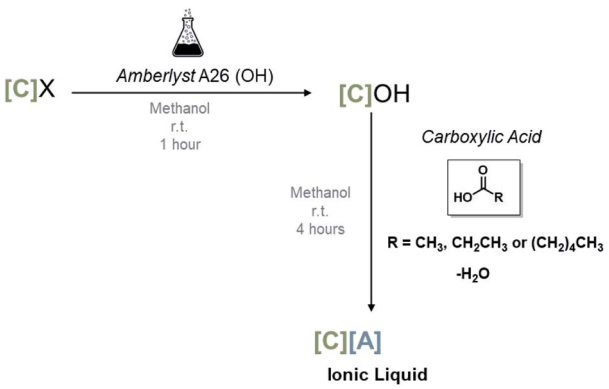

Scheme 1 General synthetic procedure to prepare the desired ionic liquids involving firstly the preparaton of the hydroxide anion throught anion exchange reaction using Amberlyst A26 (OH), followed by neutralization through acid–base reaction.

is formed in each reaction with higher relative purity levels. Take in account that both cation and anion have protons in their structures, it was possible to estimate its proportion, which seems to be closed to the expected (1 : 1). Complementary, Fourier-Transform Infrared (FTIR) spectroscopy was used to elucidate the functional groups of the commercially available salts used as starting materials and the correspondent synthesized ILs by analysis of the infrared stretching vibrations (see ESI-Fig. 13 and 14†). The FTIR-ATR spectrum of [BE]Cl showed a broad band near to 3428 cm^{-1} that can be attributed to O–H stretching vibration of water molecules present in its structure, which is broader in the case of [BE] based-ILs; a band in the range between 2987–2848 cm^{-1} that can be attributed to asymmetrical and symmetrical C–H stretching from methyl ($–CH_3$) and methylene ($–CH_2$) groups; a band near to 1513 cm^{-1} that can be assigned to aromatic ring stretching (C=C–C); a band near to 1243, 1130 and 1064 cm^{-1} that can be attributed to alkyl aryl ether, alkyl ether and C–N stretching vibrations, respectively.[57] In the case of the [BE] based-ILs showed an additional band near to 1562 cm^{-1} that can be ascribed to carboxylate symmetric stretching (C=O), indicating complete ionization of carboxylic acid and consequently, elucidation of the formation of the desired IL. In the case of [DDA]Br, the FTIR-ATR spectrum also showed a broad band near to 3420 cm^{-1} that can be attributed to O–H stretching vibration of water molecules present in its structure, which is also broader in the case of [DDA] based-ILs. Similarly, a band in the range between 2957–2853 cm^{-1} that can be attributed to asymmetrical and symmetrical C–H stretching from methyl ($–CH_3$) and methylene ($–CH_2$) groups; a band near to 1467, 900 and 722 cm^{-1} that can be assigned to CH_2 bending, out-of-plane C–H bending, in-plane rocking mode of the methylene (CH_2), respectively. In the case of [DDA] based-ILs, an additional band near to 1569 and 1390 cm^{-1} that can be ascribed to carboxylate symmetric stretching (C=O) and CH_2 bending from carboxylic acid counterpart, respectively, is observed.

Thermal analysis of the ILs

The synthesized [BE] and [DDA] based-ILs have been studied by differential scanning calorimetry (DSC) and simultaneous TGA and DSC measurements (TGA-DSC). The glass transition temperature ($T_{g\text{-mid}}$), which corresponds to the glass transition determined as mid-point, melting (T_m), crystallization (T_c), cold-crystallization (T_{cc}) and decomposition temperatures ($T_{5\%,onset}$ and $T_{d,peak}$), which $T_{5\%,onset}$ correspond when the sample lost 5% of its initial weight and $T_{d,peak}$ correspond to the temperature associated with the first step of the mass loss process are summarized in Table 1 and the respective thermograms are present in the supporting information (see ESI-Fig. 18–23 and 33–37†). The [BE]Cl is a white solid that showed a melting point around of 162.4 °C, which is closed to that one already reported in literature (see ESI-Fig. 34†).[58] The [BE][OAc] and [BE][OPr] showed only a glass transition, while [BE][OHex] showed a small tendency to crystallize in hydrated state, once an exothermic peak in the cooling run, and subsequently, a glass transition followed a small endothermic peak in heating run is observed. After complete removal of any residual solvent, all [BE]-ILs showed a glass-forming tendency, once neither crystallization nor melting were observed in the selected experimental conditions. The glass transition in dried state shift to higher temperatures according to the following sequence: T_g([BE][OAc]) > T_g([BE][OPr]) > T_g([BE][OHex]). This observation can be explained by the effect of the number of carbons in alkyl chain length of carboxylate anion. In the case of [DDA]Br, a particular thermal behaviour is observed; initially, the hydrated salt presented an amorphous region that subsequently crystallize during the heating run (cold-crystallization, T_{cc}), followed by multiples endothermic peaks that can be attributed to the melting of amorphous and crystalline fractions as well as water evaporation process. In the 3rd cooling run, [DDA]Br showed consecutive crystallization and melting transitions. This behaviour can be explained by the nature of the cation, once [DDA] is a double-chain cationic surfactant of a quaternary ammonium salt, but also its interaction with water,[59]

Table 1 Thermal properties: glass transition ($T_{g\text{-mid}}$), melting (T_m), crystallization (T_c) and cold-crystallization (T_{cc}) temperatures as well as thermal degradation temperatures ($T_{d,5\%\text{-onset}}$ and $T_{d,peak}$) of [BE]- and [DDA]-based ILs

	$DSC_{hydrated}$[a]			DSC_{dried}[b]			TGA-DSC[c]	
IL	$T_{g\text{-mid}}$ (°C)	T_c/T_m (°C)	T_{cc} (°C)	$T_{g\text{-mid}}$ (°C)	T_c/T_m (°C)	T_{cc} (°C)	$T_{d,5\%\text{-onset}}$ (°C)	$T_{d,peak}$ (°C)
[BE]Cl	—	—/162.4[d]	—	—	—/—	—	189.0	202.0
[BE][OAc]	−48.1	—/—	—	−14.4	—/—	—	146.6	163.6
[BE][OPr]	−48.0	—/—	—	−14.7	—/—	—	128.7	163.2
[BE][OHex]	−52.1	−2.5/2.4	—	−29.1	—/—	—	144.7	168.0
[DDA]Br	−73.7	—/11.7; 39.5; 83.4	−21.4	—	36.8; 15.1; −2.7; −14.7/5.9; 35.0; 68.6	—	212.1	247.3
[DDA][OAc]	−79.7	—/36.5[e]	—	−61.6	−58.0/−38.4	—	128.6	183.4
[DDA][OPr]	−78.9	—/29.4	—	−69.1	22.4/38.8	−8.9	172.6	184.8
[DDA][OHex]	−67.9	—/−2.0	−55.0; −30.8; −22.0	−76.7	6.9; −22.1/17.9; 39.0	−33.3; −3.0	167.1	187.0

[a] 1st cycle scanned at 10 °C min^{-1} (hydrated state). [b] 3rd cycle scanned at 10 °C min^{-1} (dried state). [c] $T_{d,5\%\text{-onset}}$ (onset temperature when the sample lost 5% of its initial weight) and $T_{d,peak}$ (temperature associated with the first step of the mass loss process, which were taken as the minimum of the derivative of thermogravimetric curves (DTGA)) were determined from simultaneous TGA-DSC experiments acquired from 25 °C to 500 °C at 10 °C min^{-1} under argon atmosphere. [d] Melting temperature determined from simultaneous TGA-DSC experiments. [e] Small endothermic peak overlap with water evaporation process.

leading to the formation of polymorphs.[60] According to literature, dialkyldimethylammonium bromides exhibit a liquid crystalline behaviour, where mainly two endothermic transitions can be observed and they can be ascribed to the melting of crystal into a liquid-crystalline phase at lower temperatures, followed by a clearing point.[60] It is also mentioned that the crystalline phase at low temperatures showed a complex polymorphism, where a coexisting metastable crystal form is observed.[60] The [DDA] based-ILs showed similar thermal events even in the dried state. In the hydrated state, [DDA][OAc], [DDA][OPr] and [DDA][OHex] showed similar thermal events, namely glass transition and, an endothermic peak that can be ascribe to the melting of small crystalline fraction present in the sample. In the case of [DDA][OAc] and [DDA][OPr] this melting is detected as a small endothermic peak close to a broader endothermic peak that can be ascribed to water evaporation. While, in the case of [DDA][OHex], an additional consecutives exothermic peaks in the heating run, which can be explained by the crystallization of amorphous fraction into different crystalline forms, followed by an endothermic peak, which appears at lower temperature than [DDA][OAc] and [DDA][OPr], can be observed.

Indeed, all [DDA] based-ILs showed tendency to crystallize in dried state, even the amorphous fraction, *i.e.*, observation of an exothermic peak during the heating run that can be ascribe to cold-crystallization process, except for [DDA][OAc], where the amorphous fraction did not crystallize. Similar to the [BE] based-ILs, the glass transition in dried state shift to higher temperatures according to the following sequence: T_g([DDA][OAc]) > T_g([DDA][OPr]) > T_g([DDA][OHex]). This observation can be also explained by the effect of the number of carbons in alkyl chain length of carboxylate anion.

In general, all prepared ILs showed lower thermal stability than the correspondent commercially available salts as expected for carboxylate anions.[61] In the case of the ILs, a gradual weight loss starting at lower temperatures, which can be associated to water evaporation process, is observed. In general, the ILs showed a two-step decomposition processes, lower than the correspondent starting material, and it is observed that the alkyl chain length of carboxylate anion has a minimal impact in these decomposition temperatures as expected.[61]

Development of polymeric structures

The dissolution studies consisted in the addition of an adequate amount of microcrystalline cellulose (MCC) to each IL, under constant stirring at fixed temperature for a determined time. Initially, screening experiments have been performed to determine the optimal temperature, time, and ratio between MCC and IL. In this sequence, [BE] and [DDA] based-ILs showed ability to dissolve MCC at 100 °C for 14 and 4 hours, respectively, at maximum concentration of 4% (w/w), after visual observation if there are any particles in suspension. The polymeric structures, as a film or gel form, have been developed thought water phase inversion method, depending on the ratio between MCC and IL (1 or 4% (w/w)) as well as the type of IL. Indeed, [BE]-ILs produced gels, while [DDA]-ILs produced films or gels depending on the length of alkyl chain of the anion that constituted the IL.

Fourier transform-infrared (FTIR) analysis of polymeric structures

The composition of the produced polymeric structures has been evaluated by FTIR spectroscopy and compared to pure IL and pure MCC to elucidate their presence or not in the resulting polymeric structure. According to FTIR-ATR spectrum (see ESI-Fig. 15†), MCC showed a broad band near to 3336 cm^{-1} that can be assigned to O–H stretching vibration from hydroxyl groups;[3,62,63] a band at 2894 and 1638 cm^{-1} that can be attributed to sp^3 C–H stretching vibration and –OH bonding of absorbed water, respectively;[62–64] a small band at 1429 cm^{-1} that can be attributed to intermolecular hydrogen attraction at the C6 group;[63,64] a band between 1369–1315 cm^{-1} that can be ascribe to the C–H bending and C–O symmetric stretching groups of aromatic ring present in polysaccharide;[63,64] a band that appears as a small shoulder at 1158 and 1104 cm^{-1} that can be ascribed to C–C and C–O–C glycosidic ether band, respectively;[64] a sharp band near to 1028 cm^{-1} that can be ascribe to the stretching vibration of the C–O–C pyranose ring;[63,64] a small band as a shoulder near to 897 cm^{-1} that can be ascribed to C–H rocking vibration.[64] Indeed, the region between 1100–600 cm^{-1} can be related to twisting, wagging and deformation modes of anhydro-glucopyranose, which is characteristic of β-glycosidic linkages present in cellulose structure.[63,64] In general, the obtained gels and films showed characteristic bands that can be attributed to both cation and anion structures that constituted each IL, indicating that some IL remains in the polymeric structure after water inversion phase method, except in the case of film that containing 4% (w/w) of MCC and [DDA][OAc] was used as dissolution agent (see ESI-Fig. 16 and 17†). Also, cellulose characteristics bands can be observed, but in some cases are overlapped with bands that can be ascribed to IL structure, indicating that cellulose structure are not destroyed after dissolution and further preparation of polymeric structures. However, in the case of the gel-like structures obtained using [BE][OPr] and [BE][OHex], an additional band near to 1741 and 1737 cm^{-1}, respectively, can be detected and could be assigned to ester carbonyl group,[65,66] suggesting that cellulose may have suffer side chemical reactions during the dissolution process, including decomposition.[3,67] In general, the obtained gel-like systems and films showed a broader O–H vibration stretching band as well as a slight shift to higher wavenumbers than pure cellulose, except in the case of [DDA][OAc] with 4% (w/w) of MCC. This behaviour could be explained by the dissolution and thus, regeneration processes of cellulose, once hydrogen bonding present in original cellulose structure is disrupted, and new and weaker hydrogen bonds are formed.[3,68]

Thermal analysis of polymeric structures

The thermal stability as well as thermal behaviour of the obtained gels and films have been also performed and compared with pure MCC and ILs (see ESI-Fig. 38–41†).

According to TGA, the polymeric structures showed lower thermal stability comparing with pure MCC (see Fig. 2) as expected.[69] This fact can also be related with the presence of ionic liquid inside of polymeric structure as well as the MCC dissolution and thus, regeneration processes, where the obtained

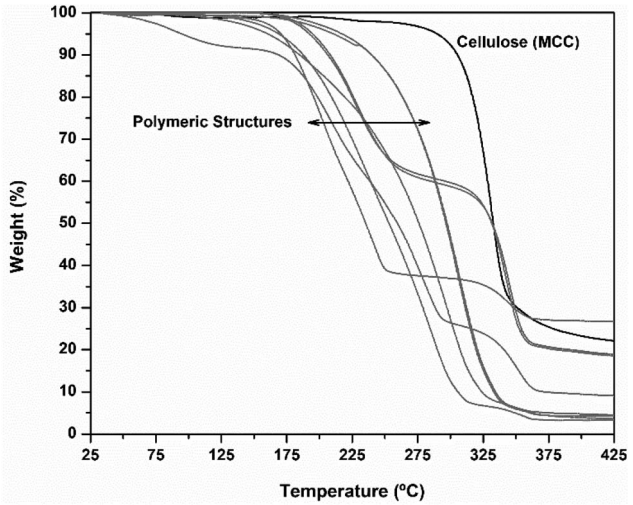

Fig. 2 Thermogravimetric curves obtained for pure MCC and respective obtained polymeric structures.

polymeric structures showed new and weaker hydrogen bonding comparing to original MCC.[3,68]

According to DSC analysis, no thermal events have been detected in the selected experimental conditions for pure MCC, after water removal (see ESI-Fig. 24†). In the case of the gel-like structures composed by [BE][OAc], [BE][OPr] and [BE][OHex], a glass transition is observed, indicating that the presence of the remained IL in polymeric structures (see ESI-Fig. 25–32†). While for [DDA][OHex], a semi-crystalline behaviour is observed, suggesting that the remained IL in the polymeric structure has also tendency to crystallize in a similar way comparing with pure IL (see ESI-Fig. 19†). According to literature, gels are considered amorphous solids with a disorder molecular organization, a finite shear viscosity, and capacity to exhibit viscoelastic stress relaxation.[70] In the case of the films, no thermal events have been detected besides solvent evaporation in the selected experimental conditions contrary to the neat ILs. A possible interpretation can be related by the fact that the presence of IL in a polymeric structure can lead to a depression on glass transition, suppression of crystallization and thus, melting at least in the temperature range explored.

Rheological studies

Rheological studies were performed to evaluate the viscoelastic properties as well as viscosity behaviour of the developed gel-like structures. The viscoelastic behaviour was evaluated using small amplitude oscillatory measurements, where a constant mechanical stress was applied for a range of frequency values, and the viscous and elastic responses were measured.[71] The elastic response is represented by the storage modulus (G'), which indicates the energy stored by the sample,[71] while the viscous response is represented by the loss modulus (G''), which indicates the energy lost by the sample during the shear process.[72] Chenite *et al.*[73] reported that the strength of the gel can be evaluated take in account the magnitude of G' as well as the difference between G' and G''. When $G' \gg G''$, the sample is considered a "strong gel"[64] and, in this case, both variables, especially G', are nearly independent of frequency over a large frequency range.[70]

In this context, stress sweep measurements were performed to determine the linear viscoelastic region for each sample, and consequently, the selection of an adequate tension to perform frequency sweep measurements. Fig. 3 shows the plot of G' and G'' as a function of frequency for each sample.

According to Fig. 3, the sample formed with 1% (w/w) of MCC containing [BE][OAc] showed loss modulus values (G'') higher than storage modulus values (G'), highly dependent on frequency within the investigated frequency range, suggesting that it is composed mainly of entangled polymer chains, indicating a behaviour of a viscous solution instead of an effective polymeric gel network. However, increasing MCC concentration to 4% (w/w) with [BE][OAc], a behaviour typically attributed to a "weak gel" is observed, once the storage modulus values (G') become higher than loss modulus values (G''), with a small difference between them (less than one order of magnitude), and both moduli are less dependent on the frequency in the investigated frequency range. This behaviour was also observed for 4% (w/w) MCC with [BE][OPr] and [BE][OHex]. It is also noted that when the frequency increases, the values of storage (G') and loss (G'') modulus tend to become closer to each other, approaching a crossover point. At lower frequency values, the elastic response (G') is dominant over the viscous response (G''), indicating a solid-like behaviour, while at higher frequencies the loss modulus (G'') gains a similar or the same importance than storage modulus (G'). This fact may be attributed to the nature (*e.g.* entanglements) and number of intermolecular interactions. By the contrary, the structure formed with 4% (w/w) of MCC containing [DDA][OHex] showed a profile of a "strong gel", once storage modulus values (G') are one order of

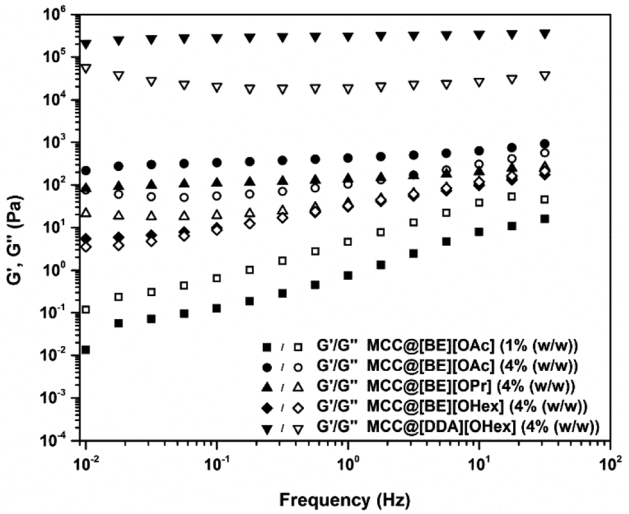

Fig. 3 Frequency sweeps of obtained MCC-based gel-like structures containing [BE][OAc], [BE][OPr], [BE][OHex] and [DDA][OHex] measured at 25 °C. The applied tension in the viscoelastic region was: 0.4 Pa for MCC@[BE][OAc] (1% (w/w)) and MCC@[BE][OHex] (4% (w/w)); 0.5 Pa for MCC@[BE][OAc] and MCC@[BE][OPr] (4% (w/w)) and 50 Pa MCC@[DDA][OHex] (4% (w/w)).

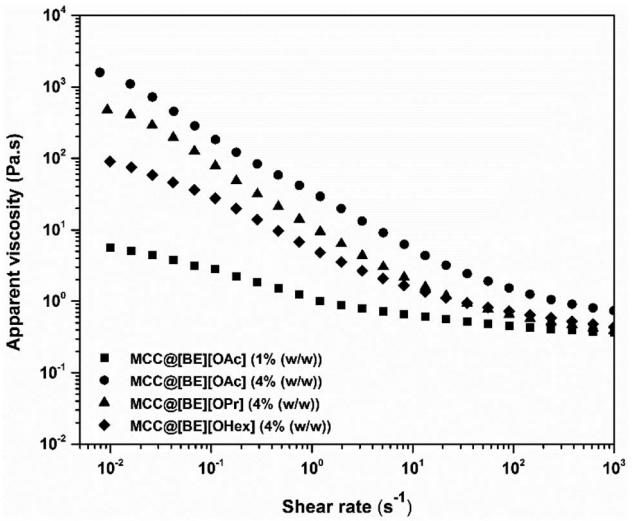

Fig. 4 Apparent viscosity as a function of shear rate for the MCC@[BE] systems measured at 25 °C.

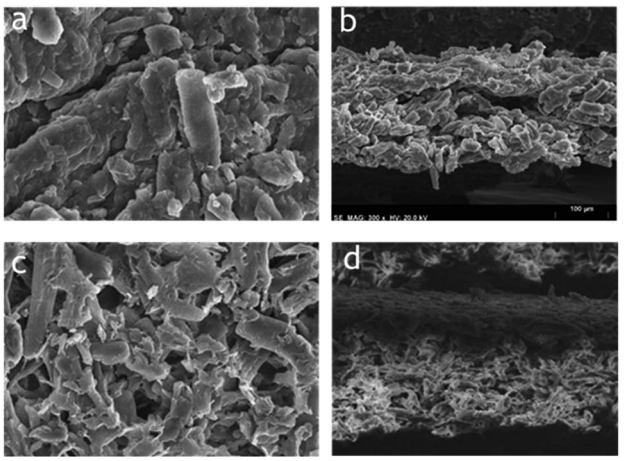

Fig. 5 SEM images of films-based MCC containing MCC@[DDA][OAc] (1% (w/w)) and MCC@[DDA][OPr] (4% (w/w)): (a) and (c) surface image (magnification of ×800), (b) and (d) a cross-section image (magnification of ×300), respectively.

magnitude higher than that of loss modulus (G''), and both of them are nearly independent of the frequency in the selected frequency range. In addition, G' and G'' values are around three orders of magnitude higher than that of MCC@[BE] systems. In fact, upon visual observation, MCC@[BE] systems with 4% (w/w) MCC presented a high consistency at rest, but with the ability to flow. As such, viscosity studies for these structures were performed (see Fig. 4). A similar profile for all tested samples is observed, where the apparent viscosity values decrease with the increase of the shear rate, a behaviour of non-Newtonian fluids with shear-thinning behaviour. Furthermore, it can be observed an increase of viscosity for the MCC@[BE][OAc] polymeric systems, when MCC concentration increased from 1% (w/w) to 4% (w/w), which is consistent with the mechanical properties shown on Fig. 3.

X-ray diffractometry (XRD)

Pure MCC and the obtained polymeric structures as films have been analysed by X-ray diffractometry (XRD) to evaluate their crystallinity. According to XRD analysis, pure MCC showed three distinct peaks at $2\theta = 15.4°$, 22.6° and 34.6° (see ESI-Fig. 42†) that can be assigned to the characteristic peaks for cellulose I crystals, which are in reasonable agreement with the values reported in the literature.[74] Indeed, the main crystalline peak is observed at $2\theta = 22.6°$, indicating the presence of crystalline cellulose, which agrees with literature.[75] The obtained films MCC@[DDA][OAc] with 1% (w/w) showed different peaks at $2\theta = 16.8°$, 20.6° as distinct shoulder, 22.5° and 34.7°; MCC@[DDA][OAc] with 4% (w/w) 15.5°, 22.7° and 34.6° and MCC@[DDA][OPr] with 4% (w/w) 15.6°, 22.6° and 34.6°. These diffraction peaks are similar to the obtained to pure MCC, suggesting that the obtained films containing cellulose I crystal without structural changes of cellulose.

Scanning electron microscopy (SEM)

The polymeric structures obtained as films, namely MCC@[DDA][OAc] with 1% (w/w) and 4% (w/w) and [DDA][OPr] 4% (w/w) were analysed by scanning electron microscopy to elucidate their morphology through analysis from its surface as well as cross-section images (see Fig. 5).

From the surface and cross-section SEM images, it is possible to observe a heterogeneous surface in the polymeric structures, which can be explained possibility due to the presence of IL in MCC network.

Experimental

Chemicals

Benzethonium chloride ([BE]Cl, TCI, >95%), didecyldimethylammonium bromide ([DDA]Br, Carbosynth, 99%), acetic acid (Honeywell, ≥99.9%), propanoic acid (Merck, ≥99%), hexanoic acid (Merck, ≥98%), Amberlyst A-26 (OH) (Sigma-Aldrich, ≥0.8 eq. L^{-1}), microcrystalline cellulose (Sigma-Aldrich, 20 μm, S3504) and methanol (Honeywell, ≥99.9%) were used as received.

General procedure for synthesis of ionic liquids

The desired ionic liquids were synthesised according to an adapted synthetic procedure already reported in the literature, which avoid the formation of inorganic salts during the ILs synthesis.[52–55] The ion-exchange resin, Amberlyst A26 (OH) (*ca.* 1.5 equivalents) was added to the halide salt of the desired cation ([BE]Cl or [DDA]Br, *ca.* 50 g) in methanolic solution and then, the suspension was stirred at room temperature for one hour. After that, the resin was removed by filtration and the corresponding hydroxide salt was slowly added to the desired carboxylic acid in methanolic solution, and subsequently, the solution was stirred at room temperature for four hours. Then, the methanol was evaporated, and the desired product was dried under vacuum.

General procedure for development of polymeric structures

Suitable amount of microcrystalline cellulose (MCC) (1 to 5% (w/w) – ratio between polymer and IL) was slowly added to IL (15

g) previously heated at 100 °C in silicone oil bath. The mixture was continuously stirred (*ca.* 400 rpm) at 100 °C for 4 or 14 hours, depending on the type of IL. After that, the mixture was casted into a glass substrate, and a casting knife with pre-defined thickness between 150–200 μm have been applied, and then, immersed in water as non-solvent in coagulation bath at room temperature, for 24 hours. Afterwards, the obtained polymeric structure was left to dry at room temperature for 1–2 weeks.

NMR spectroscopy

NMR spectra were done on a Bruker AMX 400 instrument operating at 400.13 MHz (^{1}H), 100.61 MHz (^{13}C). The NMR spectrometers are part of The National NMR Facility supported by Fundação para a Ciência e a Tecnologia (RECI/BBB-BQB/0230/2012).

FTIR-ATR spectroscopy

Fourier transform infrared spectroscopy (FTIR) was carried out using a PerkinElmer Spectrum Two™, equipped with ATR accessory. The spectra were acquired between 4000–400 cm^{-1} with 10 scans of accumulation.

Simultaneously TGA-DSC experiments

Simultaneously TGA-DSC experiments (TGA-DSC) was performed on a Setaram Labsys EVO, where the samples are continuously purged with an argon flow of 50 mL min^{-1} from 25 °C to 500 °C at 10 °C min^{-1}.

DSC measurements

DSC analysis is carried out using a TA Instruments Q-series TM Q2000 DSC with a refrigerated cooling system (RCS 90). About 4–6 mg of the salt was crimped in an aluminium standard pan with lid, containing a small pinhole to allow solvent evaporation during the experiment. The sample is continuously purged with 50 mL min^{-1} of nitrogen flow and submitted to a heating/cooling rate of 10 °C min^{-1} from −90 °C to 100 or 120 °C.

SEM

Scanning electron microscopy was performed using a Hitachi model S2400 with an electron beam intensity of 20 kV and the respective micrographs from surface and cross-section of the films were acquired using Esprit 1.9 software. All tested samples were coated with a thin Pd/Au layer to induce charge under the electron beam.

Rheology tests

The viscoelastic studies of the obtained polymeric structures with a gel-like behaviour have been performed in a Haake Mars™ III, Thermo Scientific Rheometer with a corrugated plate–plate geometry with 2 cm of diameter with 0.1 cm of gap or a cone–plate geometry with a 3.5 cm of diameter, 2° for the cone angle and 0.0105 cm for the gap, depending on the physical characteristics of the sample. Stress sweeps were performed to evaluate the linear viscoelastic region, at a constant frequency of 1 Hz, and temperature of 25 °C, for a shear stress range between 0.01–1000 Pa. Subsequently, frequency sweeps between 0.01 and 100 Hz have been performed at constant tension, within the linear viscoelastic region previously determined. Apparent viscosity was measured using a stationary shear flow and recorded as a function of shear rate (0.01–1000 s^{-1}).

XRD analysis

XRD pattern was recorded using Rigaku Miniflex II X-ray diffractometer with a scanning range between $2\theta = 3°$ to 60° at room temperature with Cu X-ray radiation (30 kV/15 mA).

Conclusions

In conclusion, it was described for the first time the synthesis and further, application of dual functional ionic liquids that may have biological properties as biopolymer dissolution agent to develop polymeric structures, which can be advantageous when some IL remain in polymeric structures after phase inversion method.

In this work, benzethonium and didecyldimethylammonium based-ILs have been successful synthesized after combination with short alkyl carboxylate anions being confirmed by ^{1}H and ^{13}C NMR, FTIR-ATR spectroscopies and elemental analysis. After optimized the dissolution conditions, it was observed that all tested ILs have been able to dissolve MCC up to a concentration of 4% (w/w), resulting in different polymeric structures as gel-like or film depending on the type of IL and ratio between MCC and IL. Also, according to FTIR spectroscopy, the obtained gel-like and films structures showed that some IL remains in the polymeric structures, which can enhance their application in the biomedical field.

Author contributions

Joana Galamba – investigation and methodology; Vítor D. Alves – investigation and methodology; Noémi Jordão – conceptualization, investigation, methodology, supervision and writing – original draft, review & editing; Luísa A. Neves – conceptualization, funding acquisition, project administration, resources, supervision and writing – review & editing.

Conflicts of interest

There are no conflicts to declare.

Acknowledgements

This work was supported by the Associate Laboratory for Green Chemistry – LAQV which is financed by national funds from FCT/MCTES (UIDB/50006/2020 and UIDP/50006/2020); Linking Landscape, Environment, Agriculture and Food Research Centre (LEAF), which is financed by national funds from FCT/MCTES (UID/AGR/04129/2020) and the national project "PTDC/CTM-CTM/29869/2017", which is financed by Fundação para a Ciência e a Tecnologia (FCT). The NMR spectrometers are part of The National NMR Facility, supported by FCT/MCTES (RECI/BBB-BQB/0230/2012).

Notes and references

1 E. S. Morais, A. M. da Costa Lopes, M. G. Freire, C. R. Freire, J. A. P. Coutinho and A. J. D. Silvestre, *Molecules*, 2020, **25**, 3652.
2 S. Gao, G. Tang, D. Hua, R. Xiong, J. Han, S. Jiang, Q. Zhang and C. Huang, *J. Mater. Chem. B*, 2019, **7**, 709–729.
3 J. Yang, X. Lu, X. Yao, Y. Yang, Q. Zhou and S. Zhang, *Green Chem.*, 2019, **21**, 2777–2787.
4 H. Wang, G. Gurau and R. D. Rogers, *Chem. Soc. Rev.*, 2012, **41**, 1519–1537.
5 M. T. Cough, K. Geyer, P. A. Hunt, S. Son, U. Vagt and T. Welton, *Green Chem.*, 2015, **17**, 231–243.
6 B. Zheng, C. Harris, S. R. Bhatia and M. F. Thomas, *Polym. Adv. Technol.*, 2019, **30**, 1751–1758.
7 M. Brehm, J. Radicke, M. Pulst, F. Shaabani, D. Sebastiani and J. Kressler, *Molecules*, 2020, **25**, 3539.
8 A. Xu and F. Wang, *Green Chem.*, 2020, **22**, 7622–7664.
9 F. Hermanutz, F. Gähr, E. Uerdingen, F. Meister and B. Kosan, *Macromol. Symp.*, 2010, **262**, 23–27.
10 H. P. Fink, P. Weigel, H. J. Purz and J. Ganster, *Prog. Polym. Sci.*, 2001, **26**, 1473–1524.
11 T. Heinze and T. Liebert, *Prog. Polym. Sci.*, 2001, **26**, 1689–1762.
12 C. L. McCormick and T. R. Dawsey, *Macromolecules*, 1990, **23**, 3606–3610.
13 S. Fischer, W. Voigt and K. Fischer, *Cellulose*, 1999, **6**, 213–219.
14 Z. Wang, T. Yokoyama and H. M. Chang, *Food Chem.*, 2009, **57**, 6167–6170.
15 H. S. Qi, J. Cai, L. N. Zhang and S. G. Kuga, *Biomacromolecules*, 2009, **10**, 1597–1602.
16 D. Ruan, L. Zhang, J. Zhou, H. Jin and H. Chen, *Macromol. Biosci.*, 2004, **4**, 1105–1112.
17 J. F. Wang, Z. M. Xue, C. Y. Yan, Z. H. Li and T. C. Mu, *Phys. Chem. Chem. Phys.*, 2016, **18**, 32772–32779.
18 R. P. Swatloski, S. K. Spear, J. D. Holbrey and R. D. Rogers, *J. Am. Chem. Soc.*, 2002, **124**, 4974–4975.
19 O. Stolarska, A. Pawłowska-Zygarowicz, A. Soto, H. Rodríguez and M. Smiglak, *Carbohydr. Polym.*, 2017, **178**, 277–285.
20 S. Zhu, Y. Wu, Q. Chen, Z. Yu, C. Wang, S. Jin, Y. Ding and G. Wu, *Green Chem.*, 2006, **8**, 325–327.
21 H. Zhang, J. Wu, J. Zhang and J. He, *Macromolecules*, 2005, **38**(20), 8272–8277.
22 J. Zhang, J. Wu, J. Yu, X. Zhang, J. He and J. Zhang, *Mater. Chem. Front.*, 2017, **1**, 1273–1290.
23 F. Liu, Z. Xue, X. Zhao, H. Mou, J. He and T. Mu, *Chem. Commun.*, 2018, **54**, 6140–6143.
24 H. Zhang, J. Lang, P. Lan, H. Yang, J. Lu and Z. Wang, *Materials*, 2020, **13**, 278.
25 Y. L. Chen, X. Zhang, T. T. You and F. Xu, *Cellulose*, 2019, **26**, 205–213.
26 S. Sen, J. D. Martin and D. S. Argyropoulos, *ACS Sustainable Chem. Eng.*, 2013, **1**, 858–870.
27 M. Kostag, M. Gericke, T. Heinze and O. A. El Seoud, *Cellulose*, 2019, **26**, 139–184.
28 T. Heinze and M. Gericke, Ionic Liquids as Solvents for Homogeneous Derivatization of Cellulose: Challenges and Opportunities, in *"Production of Biofuels and Chemicals with Ionic Liquids", Biofuels and Biorefineries*, ed. Z. Fang, R. Smith Jr and X. Qi, Springer, Dordrecht, 2014, vol. 1.
29 J. L. Anthony, J. F. Brennecke, J. D. Holbrey, E. J. Maginn, R. A. Mantz, R. D. Rogers, P. C. Trulove, A. E. Visser and T. Welton, in *Ionic Liquids in Synthesis*, Wiley-VCH Verlag GmbH & Co. KGaA, 2003.
30 H. Ohno, in *Electrochemical Aspects of Ionic Liquids*, John Wiley & Sons, Inc., 2005, pp. 1–3.
31 N. V Plechkova and K. R. Seddon, *Chem. Soc. Rev.*, 2008, **37**, 123–150.
32 A. Brandt, J. Gräsvik, J. P. Hallett and J. T. Welton, *Green Chem.*, 2013, **15**, 550–583.
33 R. P. Swatloski, S. K. Spear, J. D. Holbrey and R. D. Rogers, *J. Am. Chem. Soc.*, 2002, **124**, 4974–4975.
34 L. C. Tomé, M. G. Freire, L. P. N. Rebelo, A. J. D. Silvestre, C. P. Neto, I. M. Marrucho and C. S. R. Freire, *Green Chem.*, 2011, **13**, 2464.
35 J. Wu, J. Zhang, H. Zhang, J. He, Q. Ren and M. Guo, *Biomacromolecules*, 2004, **5**, 266–268.
36 J. Li, H. Zhang, G. G. Sacripante, D. J. W. Lawton, H. S. Marway and M. R. Thompson, *Cellulose*, 2021, **28**, 1055–1069.
37 K. C. Badgujar and B. M. Bhanage, *Bioresour. Technol.*, 2015, **178**, 2–18.
38 Y. Li, J. Wang, X. Liu and S. Zhang, *Chem. Sci.*, 2018, **9**, 4027–4043.
39 M. Kimura, Y. Shinohara, J. Takizawa, S. Ren, K. Sagisaka, Y. D. Lin, Y. Hattori and J. P. Hinestroza, *Sci. Rep.*, 2015, **5**, 16266.
40 A. Hufendiek, A. Carlmark, M. A. R. Meier and C. Barner-Kowollik, *ACS Macro Lett.*, 2016, **5**, 139–143.
41 C. D. Tran and T. M. Mututuvari, *Langmuir*, 2015, **31**, 1516–1526.
42 Z. Liu, H. S. Wang, C. Liu, Y. J. Jiang, G. Yu, X. D. Mu and X. Y. Wang, *Chem. Commun.*, 2012, **48**, 7350–7352.
43 N. Husing and U. Schubert, *Angew. Chem.*, 1998, **37**, 22–45.
44 M. M. Xu, Q. B. Huang, X. H. Wang and R. C. Sun, *Ind. Crops Prod.*, 2015, **70**, 56–63.
45 Q. Y. Mi, S. R. Ma, J. Yu, J. S. He and J. Zhang, *ACS Sustainable Chem. Eng.*, 2016, **4**, 656–660.
46 F. B. Lv, C. X. Wang, P. Zhu and C. J. Zhang, *Cellulose*, 2014, **21**, 4405–4418.
47 M. Soheilmoghaddam, G. Sharifzadeh, R. H. Pour, M. U. Wahit, W. T. Whye and X. Y. Lee, *Mater. Lett.*, 2014, **135**, 210–213.
48 F. Deng, L. H. Fu and M. G. Ma, *Carbohydr. Polym.*, 2015, **121**, 163–168.
49 M. Mashkour, M. Tajvidi, F. Kimura, H. Yousefi and T. Kimura, *ACS Appl. Mater. Interfaces*, 2014, **6**, 8165–8172.
50 A. Wang, S. Li, H. Chen, Y. Hu and X. Peng, *Cellulose*, 2019, **26**, 6849–6859.
51 S. Zhang, X. Zhuang, D. Chen, F. Luan, T. He, C. Tian and L. Chen, *Microchim. Acta*, 2019, **186**, 450.

52 N. Jordão, P. Ferreira, H. Cruz, A. J. Parola and L. C. Branco, *ChemPhotoChem*, 2019, **3**, 525–528.
53 P. Ossowicz, E. Janus, M. Blaszak, K. Zaton and Z. Rozwadowski, *Tenside, Surfactants, Deterg.*, 2017, **54**, 500–509.
54 E. Alcalde, I. Dinarès, A. Ibáñez and N. Mesquida, *Molecules*, 2012, **17**, 4007–4027.
55 E. Alcalde, I. Dinares, A. Ibanez and N. Mesquida, *Chem. Commun.*, 2011, **47**, 3266–3268.
56 G. Takeoka, L. Dao, R. Y. Wong, R. Lundin and N. Mahoney, *J. Agric. Food Chem.*, 2001, **49**(7), 3316–3320.
57 M. Patil, P. Mhaldar, V. Mahadik and D. M. Pore, *Tetrahedron Lett.*, 2020, **61**, 152015.
58 M. A. Liebert, *Int. J. Toxicol.*, 1985, **4**, 65–106.
59 W. L. Hough-Troutman, M. Smiglak, S. Griffin, W. M. Reichert, I. Mirska, J. Jodynis-Liebert, T. Adamska, J. Nawrot, M. Stasiewicz, R. D. Rogers and J. Pernak, *New J. Chem.*, 2009, **33**, 26–33.
60 M. Godlewska, S. Wróbel, B. Borzęcka-Prokop, M. Michalec and P. Dynarowicz, *Mol. Cryst. Liq. Cryst.*, 1997, **300**, 113–126.
61 M. T. Clough, K. Geyer, P. A. Hunt, J. Mertes and T. Welton, *Phys. Chem. Chem. Phys.*, 2013, **15**, 20480.
62 M. Babick, M. Wozniak, K. Dwiecki, S. Borysiak and I. Ratajczak, *Molecules*, 2020, **25**, 1544.
63 X. Y. Tan, S. B. A. Hamid and C. W. Lai, *Biomass Bioenergy*, 2015, **81**, 584–591.
64 M. Haafiz, A. Hassan, Z. Zakaria and I. Inuwa, *Carbohydr. Polym.*, 2014, **103**, 119–125.
65 T. Kakko, A. W. T. King and I. Kilpeläinen, *Cellulose*, 2017, **24**, 5341–5354.
66 P. D. María and A. Martinsson, *Analyst*, 2009, **134**, 493–496.
67 E. Ohno and H. Miyafuji, *J. Wood Sci.*, 2014, **60**, 428–437.
68 D. G. Raut, O. Sundman, W. Su, P. Virtanen, Y. Sugano, K. Kordas and J.-P. Mikkola, *Carbohydr. Polym.*, 2015, **130**, 18–25.
69 N. Muhammad, Z. Man, M. A. B. Khalil, I. M. Tan and S. Maitra, *Waste Biomass Valorization*, 2010, **1**, 315–321.
70 J. F. Douglas, *Gels*, 2018, **4**, 19.
71 J. D. Ferry, in *Viscoelastic Properties of Polymers*, Wiley, 3rd edn, 1980.
72 A. N. Jătariu (Cadinoiu), M. Danu, C. A. Peptu, G. Ioanid, C. Ibanescu and M. Popa, *Soft Mater.*, 2013, **11**, 45–54.
73 A. Chenite, M. Buschmann, D. Wang, C. Chaput and N. Kandani, *Carbohydr. Polym.*, 2001, **46**, 39–47.
74 S. Bano and Y. S. Negi, *Carbohydr. Polym.*, 2017, **157**, 1041–1049.
75 C. Trilokesh and K. B. Uppuluri, *Sci. Rep.*, 2019, **9**, 16709.